

Geometric wavefront dislocations of RKKY interaction in grapheneShu-Hui Zhang ^{1,*}, Jin Yang,² Ding-Fu Shao ³, Wen Yang,^{2,†} and Kai Chang^{4,5,6,‡}¹*College of Mathematics and Physics, Beijing University of Chemical Technology, Beijing 100029, China*²*Beijing Computational Science Research Center, Beijing 100193, China*³*Department of Physics and Astronomy and Nebraska Center for Materials and Nanoscience, University of Nebraska, Lincoln, Nebraska 68588-0299, USA*⁴*SKLSM, Institute of Semiconductors, Chinese Academy of Sciences, P.O. Box 912, Beijing 100083, China*⁵*CAS Center for Excellence in Topological Quantum Computation, University of Chinese Academy of Sciences, Beijing 100190, China*⁶*Beijing Academy of Quantum Information Sciences, Beijing 100193, China*

(Received 17 September 2021; accepted 24 November 2021; published 6 December 2021)

Magnetically doped graphene has great potential for applications in spintronics, in which local magnetic moments are coupled by the Rudermann-Kittel-Kasuya-Yosida (RKKY) interaction. RKKY interaction in graphene has attracted intensive interest. However, previous studies only show the features of the RKKY interaction dictated by energy dispersion, leaving the effect of the geometric nature of electronic structures unexplored. Here, we focus on the short-range oscillation behaviors of RKKY interaction contributed by intervalley scattering. Due to the unique geometric nature of electronic structures, two wavefront dislocations emerge in the RKKY interaction corresponding to winding number 1 of graphene. We further demonstrate the robustness of wavefront dislocations against the doping, trigonal warping, and gap opening of energy bands. This study reveals a unique feature for the RKKY interaction and implies the importance of the geometric nature of electronic structures for magnetism.

DOI: [10.1103/PhysRevB.104.245405](https://doi.org/10.1103/PhysRevB.104.245405)**I. INTRODUCTION**

Graphene, due to its unique electronic structure, exhibits novel physical properties and has great potential applications [1]. Graphene-based spintronics is very promising due to the long spin relaxation and decoherence time [2]. However, intrinsic graphene is nonmagnetic, which hinders its application in spintronics. One way to surmount this obstacle is to introduce the magnetic moments into graphene [3], e.g., through the carbon vacancy [4] or substitutional magnetic atoms [5,6]. Usually, the introduced magnetic moments are away from each other and have no direct coupling, but they can be coupled indirectly by the propagation and interference of itinerant carriers in graphene, i.e., the Rudermann-Kittel-Kasuya-Yosida (RKKY) interaction [7–9]. The RKKY interaction plays a crucial role in fundamental physics and realistic applications, e.g., it is responsible for the formation of different magnetic phases in diluted magnetic systems [10] and is the underlying mechanism for applications in spintronics [11–13] and scalable quantum computation [14,15]. Such importance makes the RKKY interaction a central topic in the field of graphene since its discovery [16–36].

The intensive studies demonstrate some main features of RKKY interaction in uniform graphene, which are caused by two factors, i.e., system dimension and energy disper-

sion [3]. The RKKY interaction in a two-dimensional system should have an R^{-2} decay rate with R being the impurity spacing. In doped graphene, the RKKY interaction assumes the expected decay and oscillates in the period of a half Fermi wavelength which originates from the energy dispersion [23]. In undoped graphene, the linear energy dispersion with electron-hole symmetry dictates the very remarkable RKKY interaction such as the R^{-3} decay rate and the sublattice dependence (ferromagnetic/antiferromagnetic interaction between moments on the same/opposite sublattice sites) [18]. Except for the unique energy dispersion, the electronic structure of graphene possesses geometric ingredients, e.g., the Berry phase π in gapless graphene [1] or the invariant winding number 1 in gapless and gapped graphene [37]. The geometric quantities underlie a lot of exotic phenomena in graphene such as Klein tunneling [38,39] and the unconventional quantum Hall effect [40–42]. However, it is not clear how the geometric nature of the electronic structure acts on the RKKY interaction, which is a fundamental question for graphene-based spintronics.

With the wave propagation and interference, singular wave defects may occur, namely, wavefront dislocations [43]. Wavefront dislocations inherit the singularity of a wave field, at which the wave amplitude vanishes, leading to an indetermination of the phase [43]. Since the seminal discovery [43], they have become a fundamental and ubiquitous wave phenomenon possible in any wave field [44]. Recently, they have been observed by two experiments [45,46] in Friedel oscillations induced by the vacancy in graphene. We call them geometric wavefront dislocations (GWDs) since they are

* shuhui Zhang@mail.buct.edu.cn

† wenyang@csrc.ac.cn

‡ kchang@semi.ac.cn

explained by the Berry phase in gapless graphene [45,46] and/or the winding number in gapless and gapped graphene [47,48]. In light of the overlap in the physics underlying Friedel oscillations and RKKY interaction [7–9,49], i.e., the propagation and interference of itinerant carriers, we expect the emergence of GWDs in RKKY interaction. In this paper, we revisit the RKKY interaction in graphene and further focus on the intervalley scattering contribution, demonstrating the GWD and their robustness against the doping, trigonal warping, and gap opening of the energy band. As a result, we introduce a unique feature for the RKKY interaction in graphene with the geometric origin in contrast to the well-known features due to the energy dispersion, which preliminarily associates the RKKY-induced magnetism with the geometric nature of an electronic structure.

The rest of this paper is organized as follows. In Sec. II, we introduce the standard theoretical formalism for the calculations of the RKKY interaction in graphene. In Sec. III, we present our numerical results to show the emergence and robustness of GWD in intrinsic graphene (without doping and gap opening), doped graphene (without gap opening), and gapped graphene. Finally, we briefly summarize the main results of this paper in Sec. IV.

II. THEORETICAL FORMALISM

In this section, we introduce the model structure and the convention used to express the theoretical formalism for the RKKY interaction in graphene, which is rather brief since there are a lot of relevant studies [16–36].

A. Preliminary model Hamiltonian

Figure 1(a) shows the honeycomb lattice of graphene consisting of two sublattices (denoted by A and B in dashed ellipse). The tight-binding Hamiltonian of graphene is [1]

$$\hat{H}_0 = t \sum_{\langle i,j \rangle} |i, A\rangle \langle j, B| + \text{H.c.}, \quad (1)$$

where $\langle i, j \rangle$ sums over all the electron hopping between the nearest-neighbor carbon atoms, $|i, \tau\rangle$ ($\tau = A, B$) is the π_z orbital on the sublattice site τ of unit cell i . For brevity, we use the magnitude of the nearest-neighbor hopping (i.e., $t_0 = -t$ due to $t < 0$) and the lattice constant a_0 as the energy and length units from now on. One can obtain the energy dispersion through the standard Fourier transform [50], and we make the Fourier transform using the location $\{\mathbf{R}\}$ of the carbon sites,

$$|\mathbf{k}, \tau\rangle \equiv \frac{1}{\sqrt{N}} \sum_i e^{i\mathbf{k}\cdot\mathbf{R}} |i, \tau\rangle, \quad (2)$$

which transforms the basis $\{|i, \tau\rangle\}$ into the basis $\{|\mathbf{k}, \tau\rangle\}$. Thus, the Hamiltonian in momentum space has a form

$$\hat{H}_0 = \sum_{\mathbf{k}} f(\mathbf{k}) |\mathbf{k}, A\rangle \langle \mathbf{k}, B| + \text{H.c.}, \quad (3)$$

where

$$f(\mathbf{k}) = - \sum_{m=1,2,3} e^{i\mathbf{k}\cdot\mathbf{d}_m}, \quad (4)$$

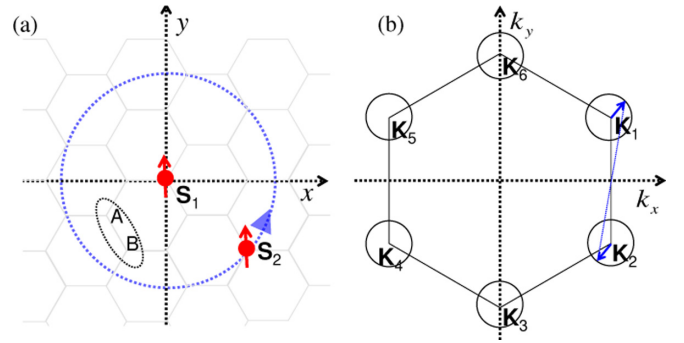


FIG. 1. Schematic RKKY interaction in graphene and the intervalley scattering contribution with the geometric origin. (a) Real-space structure of graphene with the unit cell consisting of two carbon atoms (dashed ellipse), one on sublattice A and one on sublattice B . For two local magnetic moments \mathbf{S}_1 and \mathbf{S}_2 , they couple indirectly with each other through the itinerant electron states in graphene, namely, RKKY interaction. (b) Momentum-space structure of graphene with the six famous Dirac cones \mathbf{K}_{1-6} . The RKKY interactions are mainly contributed by the backscattering events of propagating electron states between \mathbf{S}_1 and \mathbf{S}_2 . When \mathbf{S}_2 rotates around \mathbf{S}_1 in real space [blue arrow and circle in (a)], the contributing states to RKKY interaction change the momenta along the isoenergy contour, e.g., intervalley scattering between \mathbf{K}_1 and \mathbf{K}_2 in (b). As a result, the RKKY interaction should reflect the nontrivial geometric nature of electronic structure of graphene since Berry phase or winding number is defined for the circling motion of electronic states in momentum space.

and \mathbf{d}_m denotes the relative displacements of the three nearest-neighbor B sites with respect to the A sites:

$$\mathbf{d}_1 = \left(\frac{1}{2}, -\frac{\sqrt{3}}{2} \right), \quad (5a)$$

$$\mathbf{d}_2 = \left(\frac{1}{2}, \frac{\sqrt{3}}{2} \right), \quad (5b)$$

$$\mathbf{d}_3 = (-1, 0). \quad (5c)$$

To diagonalize the Hamiltonian in the momentum space, the energy dispersion is given by

$$E_{\pm}(\mathbf{k}) = \pm \sqrt{3 + 2 \cos(\sqrt{3}k_y) + 4 \cos \frac{3k_x}{2} \cos \frac{\sqrt{3}k_y}{2}}, \quad (6)$$

which presents six Dirac points at the edge of the first Brillouin zone, i.e., \mathbf{K}_{1-6} [cf. Fig. 1(b)]. Due to $\mathbf{K}_1, \mathbf{K}_3, \mathbf{K}_5$ ($\mathbf{K}_2, \mathbf{K}_4, \mathbf{K}_6$) being related to each other through a reciprocal basis vector, only two Dirac points are inequivalent, e.g., \mathbf{K}_1 and \mathbf{K}_2 , and we have

$$\mathbf{K}_1 = \frac{2\pi}{3} \left(1, \frac{1}{\sqrt{3}} \right), \quad (7a)$$

$$\mathbf{K}_2 = \frac{2\pi}{3} \left(1, -\frac{1}{\sqrt{3}} \right). \quad (7b)$$

Around the Dirac points, we can define the winding number [37]

$$W_C \equiv \oint_C \frac{d\theta}{2\pi} = 1, \quad (8)$$

with

$$\theta = -\arg f(\mathbf{k}). \quad (9)$$

In graphene, the winding number always equals 1 for the electronic states of the whole energy band, even there is one gap [37]. So, the winding number is one more intrinsic quantity than Berry phase π in gapless graphene when the low-energy linear dispersion is considered. We have identified the winding number as the underlying mechanism of robust GWDs of Friedel oscillations in gapped graphene [47,48]. Based on this deep understanding, we expect the emergency of GWDs of RKKY interaction in graphene.

B. RKKY interaction

The RKKY interaction is the usual long-range coupling among the local magnetic moments in the diluted doped host system [10]. To consider two local moments $\hat{\mathbf{S}}_{1,2}$ at $\mathbf{R}_{1,2}$ [cf. Fig. 1(a)], they couple to the carrier spin density $\hat{\mathbf{s}}(\mathbf{x}) = \hat{\mathbf{s}}(\hat{\mathbf{r}} - \mathbf{x})$, respectively, via the s - d exchange interaction $-\lambda \sum_{l=1,2} \hat{\mathbf{S}}_l \cdot \hat{\mathbf{s}}(\mathbf{R}_l)$ with λ the coupling strength. Then, each local moment can excite the spin density fluctuation of the itinerant carriers, whose propagation between $\hat{\mathbf{S}}_{1,2}$ realize their indirect coupling, i.e., RKKY interaction [7–9]. At zero temperature, the RKKY interaction $\hat{H}_{\text{RKKY}} = \sum_{\alpha,\beta=x,y,z} J_{\alpha\beta} \hat{\mathbf{S}}_{1,\alpha} \hat{\mathbf{S}}_{2,\beta}$ is characterized by the RKKY tensor [51–53]

$$J_{\alpha\beta}(E_F) = -\frac{\lambda^2}{\pi} \int_{-\infty}^{E_F} \text{Im Tr}_{\text{spin}} G(\mathbf{R}_1, \mathbf{R}_2, \varepsilon) \hat{\delta}_\beta \\ \times G(\mathbf{R}_2, \mathbf{R}_1, \varepsilon) \hat{\delta}_\alpha d\varepsilon, \quad (10)$$

which is determined by the Green's function (GF) or propagator $G(\mathbf{R}_2, \mathbf{R}_1, \varepsilon) \equiv \langle \mathbf{R}_2 | (\varepsilon + i0^+ - \hat{H}_0)^{-1} | \mathbf{R}_1 \rangle$ of the carriers between the localized spins. For the system without spin-orbit coupling, e.g., the graphene considered in this paper, the RKKY interaction assumes the Heisenberg form $\hat{H}_{\text{RKKY}} = J_{\tau\tau'} \hat{\mathbf{S}}_1 \cdot \hat{\mathbf{S}}_2$, where the scalar range function is

$$J_{\tau\tau'}(E_F, \mathbf{R}) = -\frac{\lambda^2}{2\pi} \int_{-\infty}^{E_F} d\varepsilon \text{Im } G_{\tau\tau'}^2(\mathbf{R}_2, \mathbf{R}_1, \varepsilon). \quad (11)$$

To arrive at Eq. (11), the time-reversal symmetry dictating $G_{\tau\tau'}(\mathbf{R}_1, \mathbf{R}_2, \varepsilon) = G_{\tau'\tau}(\mathbf{R}_2, \mathbf{R}_1, \varepsilon)$ has been used [52]. Here, $\mathbf{R} = \mathbf{R}_2 - \mathbf{R}_1$, and $\tau, \tau' = A$ or B are implicitly determined by $\mathbf{R}_{1,2}$ of $\hat{\mathbf{S}}_{1,2}$. According to Eq. (11), the key is to calculate the GF. For the calculation of the GF, we have developed an efficient wave function approach [54], which fully utilizes the translational invariant symmetry of the host system and reduces the calculation of the two-dimensional GF into the one-dimensional analytical GF plus one integral over the periodic momentum. Our numerical approach supports the long-range calculations of RKKY interaction needed for the filtered Fourier transform as shown in the next section. Note that one possible alternative approach to tackle the massive amount of numerical calculations is presented in one recent paper [55] and is developed in the same spirit as ours. In this paper, we focus on the RKKY interaction contributed by the intervalley scattering, so the filtered Fourier transform is needed, which can be separated into two steps. First, $J_{\tau\tau'}(E_F, \mathbf{R})$ is transformed from real space into momentum

space:

$$J_{\tau\tau'}(E_F, \mathbf{k}) = \sum_{\mathbf{R}} e^{-i\mathbf{k}\cdot\mathbf{R}} J_{\tau\tau'}(E_F, \mathbf{R}). \quad (12)$$

To obtain the numerical convergence, \mathbf{R} should be large enough, in particular, when $J_{\tau\tau'}(E_F, \mathbf{R})$ oscillates. Second, we perform the inverse transform:

$$J_{\tau\tau'}(E_F, \mathbf{R}) = \frac{1}{N_{\mathbf{k}}} \sum_{\mathbf{k} \in \mathbf{k}_{\text{filter}}} e^{i\mathbf{k}\cdot\mathbf{R}} J_{\tau\tau'}(E_F, \mathbf{k}). \quad (13)$$

Here, the summation is over momentum \mathbf{k} in the limited region $\mathbf{k}_{\text{filter}}$ including $N_{\mathbf{k}}$ points. For example, $\mathbf{k}_{\text{filter}}$ comprises two nonzero regions around two central momenta $\pm(\mathbf{K}_2 - \mathbf{K}_1)$ when one considers the intervalley scattering between valleys \mathbf{K}_2 and \mathbf{K}_1 .

III. RESULTS AND DISCUSSIONS

As a significant underlying mechanism for graphene-based spintronics, the RKKY interaction has attracted wide interest and a lot analytical and numerical efforts have been made [16–36]. In this section, we revisit the RKKY interaction in graphene and focus on the intervalley scattering contribution.

Before presenting the numerical results, we qualitatively discuss the existence of the GWD in the RKKY interaction. The wavefront dislocations as a ubiquitous wave phenomenon may occur in any wave field [44]. In particular, they are observed in Friedel oscillations in graphene on which the vacancy is intentionally introduced [45,46]. We expect the existence of GWD in the RKKY interaction based on two reasons. On one hand, Friedel oscillations and the RKKY interaction share the identical physics, i.e., the propagation and interference of electron waves of the host system, which qualitatively ensures the emergency of GWD. Second, Friedel oscillations and the RKKY interaction are both two-point responses of the host system. In the former, the two-point measurement is realized by one vacancy plus the tip of scanning tunneling microscopy (STM) while it is through two local magnetic moments in the later. Thus, if we shift one local moment around the other fixed local moment, in analogy to scanning the tip of STM around the fixed vacancy to measure Friedel oscillations, we expect the possible emergence of GWD in the RKKY interaction. In addition, the observation of GWDs in Friedel oscillations depends on the relative sublattice sites on which the vacancy and the tip of STM place. Thus the RKKY interaction between two moments on the same sublattices should differ significantly from that on the opposite sublattices. The qualitative emergence of GWD are also favored by the analytical formulas of the RKKY interaction (see the Appendix for the relevant derivations), e.g., the GWD in Friedel oscillations are shown by plotting the intervalley scattering parts of the analytical formulas on the artificial continuous points [45,46]. The Appendix is applicable to intrinsic, doped, and/or gapped graphene in the linear dispersion regime. However, realistic experiments are performed on the discrete sites and the doping may go beyond the linear dispersion of graphene. Subsequently, we numerically demonstrate the emergence and/or robustness of the GWD for the RKKY interaction in intrinsic graphene, in

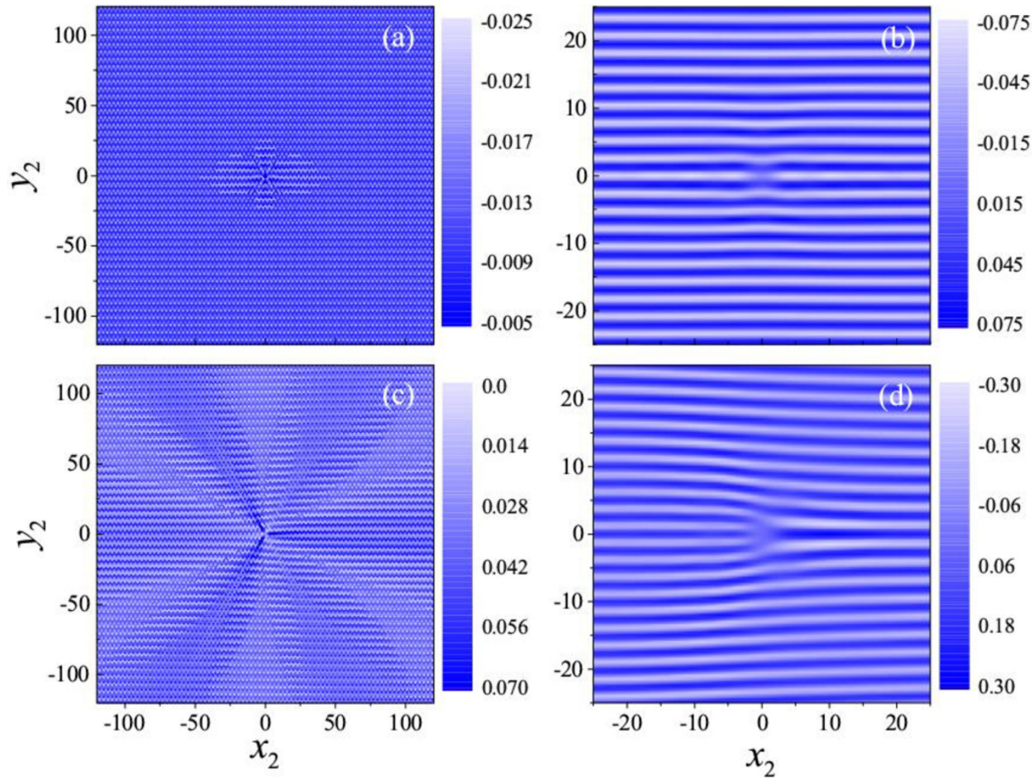


FIG. 2. The range function of RKKY interaction in intrinsic graphene (without gap opening and doping) and geometric wavefront dislocations. (a), (b) [(c), (d)] for J_{AA} (J_{AB}) and its filtered Fourier transform. J_{AA} or J_{AB} features zero or two wavefront dislocations as shown in (b) or (d). Here, the range function is multiplied by R^3 to account for the decay factor R^{-3} of RKKY interaction in intrinsic graphene.

doped graphene with special attention on the trigonal warping, and in gapped graphene. We hope these numerical simulations are helpful to future experiments.

A. Intrinsic graphene

For intrinsic graphene without gap opening and doping, Fig. 2 shows the range function of RKKY interaction between two local magnetic moments. In Fig. 2 and similar figures elsewhere, we fix one local magnetic moment at the coordinate origin and scan the position $\mathbf{R}_2 = (x_2, y_2)$ of the other magnetic moment. The top (bottom) row of Fig. 2 is for J_{AA} (J_{AB}), representing the RKKY interaction between two local magnetic moments on the same (opposite) sublattice sites. Here, the range function is multiplied by R^3 to avoid the fast decay R^{-3} of RKKY interaction in intrinsic graphene [22]. In Figs. 2(a) and 2(c), the rather long-range RKKY interactions are shown for J_{AA} and J_{AB} , which are necessary to perform the further filtered Fourier transform. Figures 2(a) and 2(c) show no particular fine structure except the short-range oscillations induced by the intervalley scattering, which can also be obtained analytically with the proper cutoff technique for the energy integral in deriving the RKKY interaction. There are six Dirac cones in graphene [cf. Fig. 1(b)], which determines three different characteristic vectors corresponding to the momentum change of intervalley scattering, and three different characteristic vectors are related to each other through C_3 symmetry. Figures 2(b) and 2(d) are plotted by performing the filtered Fourier transform to Figs. 2(a) and 2(c), in which we focus on the intervalley scattering between

\mathbf{K}_1 and \mathbf{K}_2 without loss of generality, i.e., the short-range oscillating wavefronts are perpendicular to $\mathbf{K}_1 - \mathbf{K}_2$ with the period $2\pi/(\mathbf{K}_1 - \mathbf{K}_2) = 2.6a_0$. The GWDs are visible (invisible) in Fig. 2(d) [Fig. 2(b)]. The emergence of the GWD and its sublattice dependence can also be explained by the analytical formulas for J_{AA} and J_{AB} in undoped graphene (see the Appendix for the derivation of RKKY interaction for intrinsic graphene):

$$J_{AA}(E_F = 0, \mathbf{R}) \propto 1 + \cos[(\mathbf{K}_1 - \mathbf{K}_2) \cdot \mathbf{R}_2], \quad (14)$$

$$J_{AB}(E_F = 0, \mathbf{R}) \propto 1 - \cos[(\mathbf{K}_1 - \mathbf{K}_2) \cdot \mathbf{R}_2 - 2\theta_{\mathbf{R}_2}]. \quad (15)$$

Here, $\theta_{\mathbf{R}_2}$ is the azimuthal angle of \mathbf{R}_2 , which also represents the relative vector between two local magnetic moments since $\mathbf{R}_1 = 0$. \mathbf{R}_2 has the vanishing amplitude when the second magnetic moment is also at the coordinate origin, and then leads to the singularity of J_{AB} as a wave field. The GWD of the RKKY interaction in intrinsic graphene should be explained by the Berry phase π or winding number 1. Note that in intrinsic graphene, there is zero Fermi surface and no Friedel oscillations as the Fermi surface property. Therefore, the GWD in the RKKY interaction should be due to the valence band states since it includes the energy integral over the whole valence band.

B. Doped graphene

To consider the effect of doping, Fig. 3 shows the range function of RKKY interaction in doped graphene. In the light of the sublattice dependence of the GWD, we focus on J_{AB}

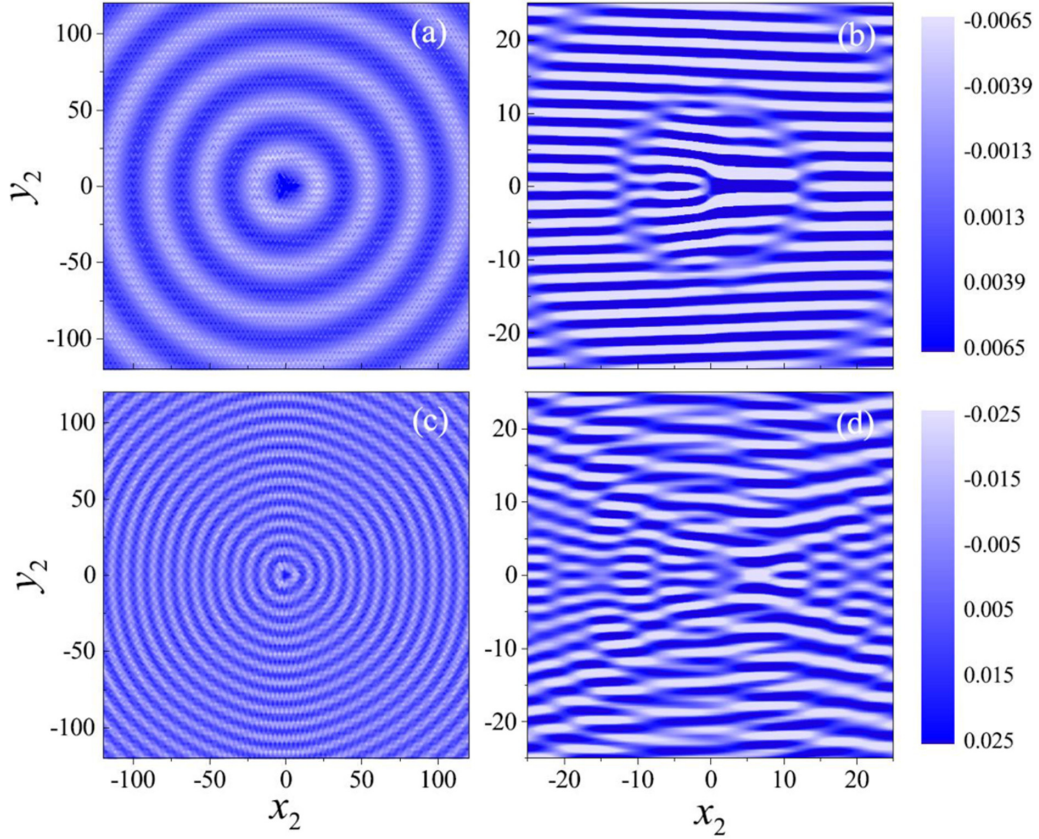


FIG. 3. The range function of RKKY interaction in doped graphene (without gap opening) and geometric wavefront dislocations. (a), (b) [(c), (d)] for J_{AB} and its filtered Fourier transform with $E_F = 0.15t_0$ ($0.5t_0$). Except the usual half Fermi wavelength oscillations, the wavefront dislocations emerge in (b) and (d) although in (d) they are blurred by the intravalley scattering induced short-range oscillations due to the short Fermi wavelength and by trigonal warping near the coordinate origin. Here, the range function is multiplied by R^2 to account for the decay factor R^{-2} of RKKY interaction in doped graphene.

later. In the top row of Fig. 3, E_F is tuned in the linear regime of energy dispersion and $E_F = 0.15t_0$ is used [1]. In Fig. 3(a), the intervalley scattering induced short-range oscillations persist as those in intrinsic graphene. The long-range oscillations occur corresponding to the intravalley scattering, and have the period of half Fermi wavelength which is $\sim \pi/k_F = \pi/(E_F/v_F) = 31.4a_0$ with $v_F = 1.5a_0t_0$. The GWD can be clearly seen in Fig. 3(b) filtered from Fig. 3(a). And the robustness of GWD against the doping in linear energy dispersion has been checked by using the other values of E_F (not shown here). In fact, the GWD in doped graphene is also assured by the analytical formula (see the Appendix for the derivation of RKKY interaction for doped graphene), i.e., $J_{AB}(E_F \neq 0, \mathbf{R}) \propto J_{AB}(E_F = 0, \mathbf{R})$ holding the singularity of $\theta_{\mathbf{R}_2}$. With increasing doping, it is well-known that the Fermi surface of graphene becomes trigonal warping [1]. Trigonal warping has a profound effect on the electron propagation in graphene, e.g., it causes the broken chirality in STM measurements [56] and modifies focusing behaviors [57–60] and perfect transmission [50] across graphene junctions. Whether trigonal warping affects the existence of GWD is not clear, even for Friedel oscillations. Due to the complexity induced by trigonal warping, the RKKY interaction and Friedel oscillations both cannot be derived analytically, which calls for numerical treatment. In the bottom row of Fig. 3, we use

$E_F = 0.5t_0$ beyond the linear energy dispersion of graphene. The GWDs persist in Fig. 3(d) but are blurred by (not the intravalley scattering) the envelop oscillations with the short wavelength corresponding to the finite Fermi surface at large doping and by trigonal warping near the coordinate origin. The blurred GWD can be highlighted through the gap opening of graphene as shown in the next section.

C. Gapped graphene

Gapped graphene has paramount importance as gapless graphene viewed from the fundamental physics [61,62] and potential applications [63]. There are many ways to achieve the gap opening of graphene, and the gap opening usually introduces different on-site potentials for two sublattice sites of graphene [64]. To be specific, we assume that the gap opening introduces the additional term $\hat{H}_\Delta = \Delta \sum_i |i, A\rangle \langle j, A| - \Delta \sum_j |j, B\rangle \langle j, B|$ to the Hamiltonian \hat{H}_0 . Our numerical approach is well applicable for gapped graphene [54]. In Fig. 4, we show the range function J_{AB} of RKKY interaction in gapped graphene. In the top row of Fig. 4, we use $E_F = 0.15t_0$ and the very actual gap value $\Delta = 0.033t_0$ [65,66]. The GWDs are clearly shown in Fig. 4(b) filtered from Fig. 4(a) as expected, since they also emerge in Friedel oscillations in gapped graphene [47,48]. In the bottom row of Fig. 4, we use

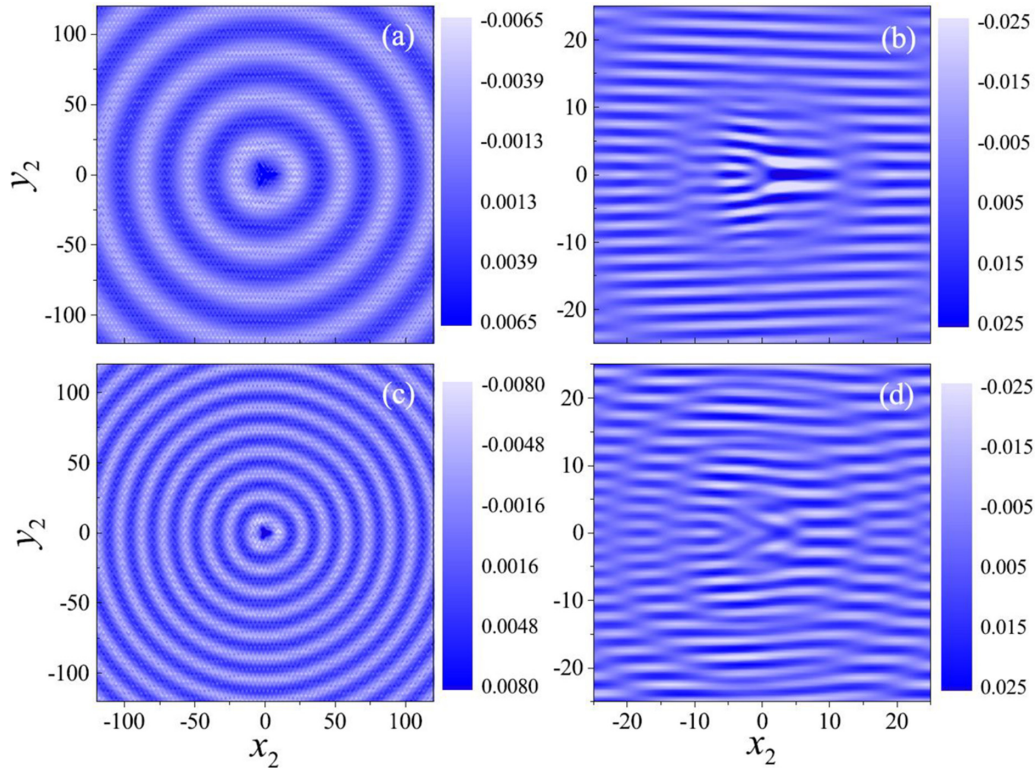


FIG. 4. The range function of RKKY interaction in gapped graphene and geometric wavefront dislocations. (a), (b) [(c), (d)] for J_{AB} and its filtered Fourier transform with $E_F = 0.15t_0$ and $\Delta = 0.033t_0$ ($E_F = 0.5t_0$ and $\Delta = 0.4t_0$). Gap opening leads to the longer half Fermi wavelength oscillations and the clear wavefront dislocations in (b) and (d), which counteracts the effect of trigonal warping in (d). Here, the range function is multiplied by R^2 to account for the decay factor R^{-2} of RKKY interaction in gapped graphene.

$E_F = 0.5t_0$ and $\Delta = 0.4t_0$. The large gap effectively deduces the Fermi wave vector, then elongates the oscillation period of RKKY interaction contributed by the intervalley scattering as shown by Fig. 4(c). Performing the filtered Fourier transform to Fig. 4(c), we obtain Fig. 4(d) which shows the clear GWD although the presence of trigonal warping of the energy band. So, the gap opening can counteract the effect of trigonal warping on the GWD.

D. Discussions

To be here, the robust GWD of RKKY interaction in graphene has been demonstrated; some discussions follow. The RKKY interaction in graphene has been studied very well [16–36] and its calculation and description are very consistent. The usual cognition is that the RKKY interaction is dictated by the energy dispersion of the electronic structure. The modern electronic structure theory surpasses the traditional energy band description [67] and is enriched by the new ingredients, e.g., the geometric nature of the electronic structure such as Berry phase and the winding number. To our knowledge, there is no relevant reference on the effect of geometrical quantities on the RKKY interaction. Here, we indeed find the interesting GWD, which may be important for the RKKY-induced magnetism in diluted magnetic systems. This paper uses graphene as an example to show the geometric effect of RKKY interaction, which is one preliminary attempt. It is more interesting to explore the geometric

effect of magnetism due to the RKKY interaction, in particular, in the system with the rich RKKY interaction terms, e.g., Dzyaloshinskii-Moriya and Ising terms occur in spin-orbit coupling systems [51,53], except the Heisenberg term in graphene.

IV. CONCLUSIONS

The RKKY interaction is a basic mechanism for magnetism and spintronics, and in graphene it attracts wide interest. Previous studies showed that the features of the RKKY interaction in graphene are dictated by the energy dispersion. For Friedel oscillations, two recent experiments [45,46] revealed the fingerprint of the geometric nature of the electronic structure, i.e., GWDs. The RKKY interaction and Friedel oscillations both originate from the propagation and interference of the electron waves, so we revisit the RKKY interaction in graphene and focus on the short-range oscillation behaviors of RKKY interaction contributed by the intervalley scattering. For the RKKY interaction in graphene, we demonstrate the emergence and/or robustness of GWDs against the doping, trigonal warping, and gap opening of energy band. In light of the successful observation of the RKKY interaction [68], we expect the observation of the wavefront dislocations of the RKKY interaction on the nanometer scale in the present experimental condition. This paper reveals a unique feature for the RKKY interaction and associates the RKKY-

induced magnetism with the geometric nature of electronic structures.

ACKNOWLEDGMENTS

This work was supported by the National Key R&D Program of China (Grant No. 2017YFA0303400), the National Natural Science Foundation of China (NSFC; Grants No. 12174019 and No. 11774021), and the NSAF grant in NSFC (Grant No. U1930402). We acknowledge the computational support from the Beijing Computational Science Research Center (CSRC).

APPENDIX: THE ANALYTICAL RKKY INTERACTION IN INTRINSIC, DOPED AND/OR GAPPED GRAPHENE

In this Appendix, we derive analytical expressions for the RKKY interaction in graphene based on the continuum model. In the low-energy continuum limit of the tight-binding model, the Hamiltonian of gapped graphene is expressed as

$$h_{\xi} = v_F(\xi\sigma_x k_x - \sigma_y k_y) + \Delta\sigma_z \quad (\text{A1})$$

by using the sublattice basis $\{A, B\}$. Here, $\xi = \pm$ denotes two inequivalent valleys $\mathbf{K}_{1,2}$ of graphene, $v_F = 3/2a_0t_0$ is the Fermi velocity, $\sigma_{x,y,z}$ is the Pauli matrix, and $\pm\Delta$ is the staggered potential on sublattices A and B induced by the breaking of the inversion symmetry. The RKKY interaction in graphene assumes the Heisenberg form $\hat{H}_{\text{RKKY}} = J_{\tau\tau'}\hat{\mathbf{S}}_1 \cdot \hat{\mathbf{S}}_2$, where the scalar range function is

$$J_{\tau\tau'}(E_F, \mathbf{R}) = -\frac{\lambda^2}{2\pi} \int_{-\infty}^{E_F} d\varepsilon \text{Im}[G_{\tau\tau'}(\mathbf{R}_2, \mathbf{R}_1, \varepsilon) \times G_{\tau'\tau}(\mathbf{R}_1, \mathbf{R}_2, \varepsilon)], \quad (\text{A2a})$$

$$= -\frac{\lambda^2}{2\pi} \int_{-\infty}^{E_F} d\varepsilon \text{Im}[G_{\tau\tau'}^2(\mathbf{R}, \varepsilon)]. \quad (\text{A2b})$$

Here, time-reversal symmetry has been used to arrive at the second line [i.e., Eq. (11) in the main text], λ is coupling strength between the local magnetic moment and the itinerant electrons, E_F is the Fermi level, and $\mathbf{R} = \mathbf{R}_2 - \mathbf{R}_1$ due to the translation invariance of the host system (namely, graphene) for the magnetic moments. For the range function calculations, the key is to derive the GF in real space. For the electron states of the energy ε , the valley-contrasting GF in real space is

$$\mathbf{G}_{\xi}(\mathbf{R}, \varepsilon) = \frac{1}{4\pi^2} \int d^2\mathbf{k} e^{i\mathbf{k}\cdot\mathbf{R}} \mathcal{G}_{\xi}(\mathbf{k}, \varepsilon). \quad (\text{A3})$$

It is the Fourier transform of the valley-contrasting GF in momentum space,

$$\mathcal{G}_{\xi}(\mathbf{k}, \varepsilon) \equiv \frac{1}{z - h_{\xi}}, \quad (\text{A4a})$$

$$= \frac{1}{z^2 - \Delta^2 - v_F^2 k^2} \begin{bmatrix} z + \Delta & \xi v_F k e^{i\xi\theta_k} \\ \xi v_F k e^{-i\xi\theta_k} & z - \Delta \end{bmatrix}, \quad (\text{A4b})$$

where $z = \varepsilon + i0^+$ with 0^+ the positive infinitesimal quantity for the retarded property of GF, and θ_k is the azimuthal angle

of the momentum \mathbf{k} . As a result, we have

$$\mathbf{G}_{\xi}(\mathbf{R}, \varepsilon) = \begin{bmatrix} -i\varepsilon_+ H_0(u) & \xi \sqrt{\varepsilon_+ \varepsilon_-} H_1(u) e^{i\xi\theta_R} \\ \xi \sqrt{\varepsilon_+ \varepsilon_-} H_1(u) e^{-i\xi\theta_R} & -i\varepsilon_- H_0^{(1)}(u) \end{bmatrix}, \quad (\text{A5})$$

where H_j is the j th order Hankel function of the first kind, $\varepsilon_{\pm} = z \pm \Delta$, $u = R\sqrt{q_+ q_-}$ with $q_{\pm} = \varepsilon_{\pm}/v_F$, and θ_R is the azimuthal angle of \mathbf{R} . Noting here θ_R in the nondiagonal elements of $\mathbf{G}_{\xi}(\mathbf{R}, \varepsilon)$ inherits from θ_k in the nondiagonal elements of $\mathbf{G}_{\xi}(\mathbf{k}, \varepsilon)$, this implies the synchronous change of θ_R in real space and θ_k in momentum space. Since θ_k is used to define the winding number [cf. Eq. (8) in the main text], the synchronous θ_R and θ_k imply the profound connection between the winding number and the real space physical quantities determined by the GF, e.g., the Friedel oscillation and the RKKY interaction. To collect the contributions of two valleys, the whole GF in real space is

$$\mathbf{G}(\varepsilon, \mathbf{R}) = \frac{1}{4v_F^2} [e^{i\mathbf{K}_1 \cdot \mathbf{R}} \mathbf{G}_+(\mathbf{R}, \varepsilon) + e^{i\mathbf{K}_2 \cdot \mathbf{R}} \mathbf{G}_-(\mathbf{R}, \varepsilon)]. \quad (\text{A6})$$

Substituting $\mathbf{G}(\varepsilon, \mathbf{R})$ into the range function, one can make the straightforward derivations as done in Refs. [22,23]. However, the usual results are not concise enough, except for intrinsic graphene ($E_F = 0$ and $\Delta = 0$), for which the range functions are

$$J_{AA}(E_F = 0, \mathbf{R}) = -\frac{\lambda^2}{128\pi v_F R^3} [1 + \cos(\Delta \mathbf{K} \cdot \mathbf{R})], \quad (\text{A7})$$

$$J_{AB}(E_F = 0, \mathbf{R}) = \frac{3\lambda^2}{128v_F \pi R^3} [1 - \cos(\Delta \mathbf{K} \cdot \mathbf{R} - 2\theta_R)]. \quad (\text{A8})$$

For the range functions $J_{AA}(E_F = 0, \mathbf{R})$ and $J_{AB}(E_F = 0, \mathbf{R})$, the first constant (second envelope) term is contributed by the intravalley (intervalley) scattering. $\Delta \mathbf{K} = \mathbf{K}_1 - \mathbf{K}_2$ is the momentum change corresponding to the intervalley scattering between valleys \mathbf{K}_1 and \mathbf{K}_2 . The analytical formulas agree with those in Ref. [22] except one numerical factor, which originates from the use of $4\pi^2$ in our Eq. (A3) but not the reduced Brillouin zone area $\Omega_{\text{BZ}} = 8\pi^2/(3\sqrt{3}a_0^2)$ of graphene in Ref. [22]. For doped and/or gapped graphene, we can also derive concise analytical formulas which are not presented in the previous references. In the long-range limit, the asymptotic expression for the Hankel function is $H_n(u) \approx \sqrt{2}/\sqrt{\pi u} e^{i(u - \frac{\pi}{2}n - \frac{\pi}{4})}$ with $n = 0, 1$ [69]. Thus, the asymptotic expression for the matrix elements of $\mathbf{G}(\varepsilon, \mathbf{R})$ are

$$G_{AA}(\varepsilon, \mathbf{R}) \approx \frac{q_+ e^{-i\frac{\pi}{4}}}{4iv_F} \sqrt{\frac{2}{\pi u}} e^{iu} (e^{i\mathbf{K}_+ \cdot \mathbf{R}} + e^{i\mathbf{K}_- \cdot \mathbf{R}}), \quad (\text{A9})$$

$$G_{BA}(\varepsilon, \mathbf{R}) \approx \frac{\sqrt{q_+ q_-} e^{-i\frac{3\pi}{4}}}{4v_F} \sqrt{\frac{2}{\pi u}} e^{iu} (e^{i\mathbf{K}_+ \cdot \mathbf{R}} e^{-i\theta_R} - e^{i\mathbf{K}_- \cdot \mathbf{R}} e^{i\theta_R}). \quad (\text{A10})$$

Using the analytical matrix elements $G_{AA}(\varepsilon, \mathbf{R})$ and $G_{BA}(\varepsilon, \mathbf{R})$, the range functions for doped and/or gapped graphene are

$$J_{AA}(E_F, \mathbf{R}) \approx -\frac{\lambda^2 (E_F + \Delta)^2 \sin\left(\frac{2R\sqrt{E_F^2 - \Delta^2}}{v_F}\right)}{16\pi^2 R^2 v_F^2 E_F} \times [1 + \cos(\Delta \mathbf{K} \cdot \mathbf{R})], \quad (\text{A11})$$

$$J_{AB}(E_F, \mathbf{R}) \approx \frac{\lambda^2(E_F^2 - \Delta^2) \sin\left(\frac{2R\sqrt{E_F^2 - \Delta^2}}{v_F}\right)}{16\pi^2 R^2 v_F^2 E_F} \times [1 - \cos(\Delta\mathbf{K} \cdot \mathbf{R} - 2\theta_R)]. \quad (\text{A12})$$

To realize the above analytical derivations, the stationary phase approximation [70] has been used, and it implies the integral over the energy for the range function is contributed mainly by the electronic states near the Fermi energy E_F , which leads to the Taylor expansion:

$$u \approx \frac{R}{v_F} \sqrt{\varepsilon_F^2 - \Delta^2} + \frac{RE_F}{v_F} (E_F^2 - \Delta^2)^{-\frac{1}{2}} (\varepsilon - E_F). \quad (\text{A13})$$

Noting here, comparing to the intrinsic case, the intravalley and intervalley terms of $J_{AA}(E_F, \mathbf{R})$ and $J_{AB}(E_F, \mathbf{R})$ both are fringed by the additional envelope oscillations. As a result, for the intrinsic, doped, and/or gapped graphene, the contribu-

tions of the intervalley scattering to the range functions have the general form

$$J_{AA}^{\text{inter}} \propto \cos(\Delta\mathbf{K} \cdot \mathbf{R}), \quad (\text{A14})$$

$$J_{AB}^{\text{inter}} \propto \cos(\Delta\mathbf{K} \cdot \mathbf{R} - 2\theta_R). \quad (\text{A15})$$

Obviously, $-2\theta_R$ in J_{AB} inherits from the GF $G_{BA}(\varepsilon, \mathbf{R})$, while it is not absent in J_{AA} since the GF $G_{AA}(\varepsilon, \mathbf{R})$ has no θ_R . The singularity of $-2\theta_R$, namely, it is indeterminate at $\mathbf{R} = 0$, leads to the emergence of the wavefront dislocations, i.e., when shifting circularly one magnetic moment at $\mathbf{R} \neq 0$ around the other fixing magnetic moment at $\mathbf{R} = 0$, the Berry phase π or winding number 1 of graphene causes an extra accumulation phase 4π , which is accommodated by two wavefront dislocations. As a result, the wavefront dislocations are visible (invisible) in J_{AB} (J_{AA}). So, the wavefront dislocations of the RKKY interaction share the same mechanism as those of Friedel oscillations [45,47].

-
- [1] A. H. Castro Neto, F. Guinea, N. M. R. Peres, K. S. Novoselov, and A. K. Geim, *Rev. Mod. Phys.* **81**, 109 (2009).
- [2] O. V. Yazyev, *Rep. Prog. Phys.* **73**, 056501 (2010).
- [3] S. R. Power and M. S. Ferreira, *Crystals* **3**, 49 (2013).
- [4] Y. Zhang, F. Gao, S. Gao, and L. He, *Sci. Bull.* **65**, 194 (2020).
- [5] E. J. G. Santos, A. Ayuela, and D. Sánchez-Portal, *New J. Phys.* **12**, 053012 (2010).
- [6] F. Donati, Q. Dubout, G. Autès, F. Patthey, F. Calleja, P. Gambardella, O. V. Yazyev, and H. Brune, *Phys. Rev. Lett.* **111**, 236801 (2013).
- [7] M. A. Ruderman and C. Kittel, *Phys. Rev.* **96**, 99 (1954).
- [8] T. Kasuya, *Prog. Theor. Phys.* **16**, 45 (1956).
- [9] K. Yosida, *Phys. Rev.* **106**, 893 (1957).
- [10] T. Jungwirth, J. Sinova, J. Mašek, J. Kučera, and A. H. MacDonald, *Rev. Mod. Phys.* **78**, 809 (2006).
- [11] S. A. Wolf, D. D. Awschalom, R. A. Buhrman, J. M. Daughton, S. von Molnar, M. L. Roukes, A. Y. Chtchelkanova, and D. M. Treger, *Science* **294**, 1488 (2001).
- [12] I. Zutic, J. Fabian, and S. Das Sarma, *Rev. Mod. Phys.* **76**, 323 (2004).
- [13] A. H. MacDonald, P. Schiffer, and N. Samarth, *Nat. Mater.* **4**, 195 (2005).
- [14] D. Loss and D. P. DiVincenzo, *Phys. Rev. A* **57**, 120 (1998).
- [15] L. Trifunovic, O. Dial, M. Trif, J. R. Wootton, R. Abebe, A. Yacoby, and D. Loss, *Phys. Rev. X* **2**, 011006 (2012).
- [16] M. A. H. Vozmediano, M. P. López-Sancho, T. Stauber, and F. Guinea, *Phys. Rev. B* **72**, 155121 (2005).
- [17] V. K. Dugaev, V. I. Litvinov, and J. Barnas, *Phys. Rev. B* **74**, 224438 (2006).
- [18] S. Saremi, *Phys. Rev. B* **76**, 184430 (2007).
- [19] L. Brey, H. A. Fertig, and S. Das Sarma, *Phys. Rev. Lett.* **99**, 116802 (2007).
- [20] E. H. Hwang and S. Das Sarma, *Phys. Rev. Lett.* **101**, 156802 (2008).
- [21] A. M. Black-Schaffer, *Phys. Rev. B* **81**, 205416 (2010).
- [22] M. Sherafati and S. Satpathy, *Phys. Rev. B* **83**, 165425 (2011).
- [23] M. Sherafati and S. Satpathy, *Phys. Rev. B* **84**, 125416 (2011).
- [24] E. Kogan, *Phys. Rev. B* **84**, 115119 (2011).
- [25] S. R. Power, P. D. Gorman, J. M. Duffy, and M. S. Ferreira, *Phys. Rev. B* **86**, 195423 (2012).
- [26] H. Lee, E. R. Mucciolo, G. Bouzerar, and S. Kettmann, *Phys. Rev. B* **86**, 205427 (2012).
- [27] J. Klinovaja and D. Loss, *Phys. Rev. B* **87**, 045422 (2013).
- [28] F. Parhizgar, R. Asgari, S. H. Abedinpour, and M. Zareyan, *Phys. Rev. B* **87**, 125402 (2013).
- [29] P. D. Gorman, J. M. Duffy, S. R. Power, and M. S. Ferreira, *Phys. Rev. B* **90**, 125411 (2014).
- [30] N. Klier, S. Shallcross, S. Sharma, and O. Pankratov, *Phys. Rev. B* **92**, 205414 (2015).
- [31] M. Agarwal and E. G. Mishchenko, *Phys. Rev. B* **95**, 075411 (2017).
- [32] J. Nokelainen, I. V. Rozhansky, B. Barbiellini, E. Lähderanta, and K. Pussi, *Phys. Rev. B* **99**, 035441 (2019).
- [33] B. Zhang, L. Jiang, and Y. Zheng, *Phys. Rev. B* **99**, 245410 (2019).
- [34] J. Cao, H. A. Fertig, and S. Zhang, *Phys. Rev. B* **99**, 205430 (2019).
- [35] A. U. Canbolat and O. Çakır, *Phys. Rev. B* **100**, 014440 (2019).
- [36] M. Ke, M. M. Asmar, and W.-K. Tse, *Phys. Rev. Research* **2**, 033228 (2020).
- [37] J. N. Fuchs, F. Piéchon, M. O. Goerbig, and G. Montambaux, *Eur. Phys. J. B* **77**, 351 (2010).
- [38] M. I. Katsnelson, K. S. Novoselov, and A. K. Geim, *Nat. Phys.* **2**, 620 (2006).
- [39] A. F. Young and P. Kim, *Nat. Phys.* **5**, 222 (2009).
- [40] K. S. Novoselov, A. K. Geim, S. V. Morozov, D. Jiang, M. I. Katsnelson, I. V. Grigorieva, S. V. Dubonos, and A. A. Firsov, *Nature (London)* **438**, 197 (2005).
- [41] Y. Zhang, Y.-W. Tan, H. L. Stormer, and P. Kim, *Nature (London)* **438**, 201 (2005).
- [42] K. S. Novoselov, E. McCann, S. V. Morozov, V. I. Fal'ko, M. I. Katsnelson, U. Zeitler, D. Jiang, F. Schedin, and A. K. Geim, *Nat. Phys.* **2**, 177 (2006).
- [43] J. F. Nye, M. V. Berry, and F. C. Frank, *Proc. R. Soc. London A* **336**, 165 (1974).

- [44] C. Dutreix, M. Bellec, P. Delplace, and F. Mortessagne, *Nat. Commun.* **12**, 3571 (2021).
- [45] C. Dutreix, H. Gonzalez-Herrero, I. Brihuega, M. I. Katsnelson, C. Chapelier, and V. T. Renard, *Nature (London)* **574**, 219 (2019).
- [46] Y. Zhang, Y. Su, and L. He, *Phys. Rev. Lett.* **125**, 116804 (2020).
- [47] S.-H. Zhang, J. Yang, D.-F. Shao, Z. Wu, and W. Yang, *Phys. Rev. B* **103**, L161407 (2021).
- [48] J. Yang, D.-F. Shao, S.-H. Zhang, and W. Yang, *Phys. Rev. B* **104**, 035402 (2021).
- [49] J. Friedel, *London, Edinburgh, Dublin Philos. Mag. J. Sci.* **43**, 153 (1952).
- [50] S.-H. Zhang and W. Yang, *Phys. Rev. B* **97**, 035420 (2018).
- [51] J.-J. Zhu, D.-X. Yao, S.-C. Zhang, and K. Chang, *Phys. Rev. Lett.* **106**, 097201 (2011).
- [52] S.-H. Zhang, J.-J. Zhu, W. Yang, and K. Chang, *2D Mater.* **4**, 035005 (2017).
- [53] S.-H. Zhang, J.-J. Zhu, W. Yang, and K. Chang, *Phys. Rev. B* **99**, 195456 (2019).
- [54] S.-H. Zhang, W. Yang, and K. Chang, *Phys. Rev. B* **95**, 075421 (2017).
- [55] M. Istas, C. Groth, and X. Waintal, *Phys. Rev. Research* **1**, 033188 (2019).
- [56] D. Dombrowski, W. Jolie, M. Petrovic, S. Runte, F. Craes, J. Klinkhammer, M. Kralj, P. Lazić, E. Sela, and C. Busse, *Phys. Rev. Lett.* **118**, 116401 (2017).
- [57] J. L. Garcia-Pomar, A. Cortijo, and M. Nieto-Vesperinas, *Phys. Rev. Lett.* **100**, 236801 (2008).
- [58] Y. Xing, J. Wang, and Q.-f. Sun, *Phys. Rev. B* **81**, 165425 (2010).
- [59] K. J. A. Reijnders and M. I. Katsnelson, *Phys. Rev. B* **96**, 045305 (2017).
- [60] S. S. R. Bladwell, *Phys. Rev. B* **101**, 045404 (2020).
- [61] F. Guinea, M. I. Katsnelson, and A. K. Geim, *Nat. Phys.* **6**, 30 (2010).
- [62] D. Xiao, W. Yao, and Q. Niu, *Phys. Rev. Lett.* **99**, 236809 (2007).
- [63] F. Schwierz, *Nat. Nanotechnol.* **5**, 487 (2010).
- [64] A. Chaves, J. G. Azadani, H. Alsalman, D. R. da Costa, R. Frisenda, A. J. Chaves, S. H. Song, Y. D. Kim, D. He, J. Zhou *et al.*, *npj 2D Mater. Appl.* **4**, 29 (2020).
- [65] S. Y. Zhou, G.-H. Gweon, A. V. Fedorov, P. N. First, W. A. de Heer, D.-H. Lee, F. Guinea, A. H. Castro Neto, and A. Lanzara, *Nat. Mater.* **6**, 770 (2007).
- [66] E. Rotenberg, A. Bostwick, T. Ohta, J. L. McChesney, T. Seyller, and K. Horn, *Nat. Mater.* **7**, 258 (2008).
- [67] D. Xiao, M.-C. Chang, and Q. Niu, *Rev. Mod. Phys.* **82**, 1959 (2010).
- [68] L. Zhou, J. Wiebe, S. Lounis, E. Vedmedenko, F. Meier, S. Blugel, P. H. Dederichs, and R. Wiesendanger, *Nat. Phys.* **6**, 187 (2010).
- [69] M. Abramowitz and I. A. Stegun, *Handbook of Mathematical Functions with Formulas, Graphs, and Mathematical Table* (Dover, New York, 1970), p. 364.
- [70] S.-H. Zhang, D.-F. Shao, and W. Yang, *J. Magn. Magn. Mater.* **491**, 165631 (2019).